Molecular-scale surface structures of oligo(ethylene glycol)-terminated self-assembled monolayers investigated by frequency modulation atomic force microscopy in aqueous solution

Molecular-Scale Surface Structures of Oligo(ethylene glycol)-Terminated Self-Assembled Monolayers Investigated by Frequency Modulation Atomic Force Microscopy in Aqueous Solution

N Inada[1], H Asakawa[2], Y Matsumoto[3] and T Fukuma[1–4]

[1] Division of Electrical and Computer Engineering, Kanazawa University, Kakuma-machi, Kanazawa 920-1192, Japan

[2] Bio-AFM Frontier Research Center, Kanazawa University, Kakuma-machi, Kanazawa 920-1192, Japan

[3] Department of Chemistry, Kyoto University, Kyoto 606-8502, Japan

[4] ACT-C, Japan Science and Technology Agency, Honcho 4-1-9, Kawaguchi 332-0012, Japan

E-mail: fukuma@staff.kanazawa-u.ac.jp

Abstract. The structure and protein resistance of oligo(ethylene glycol)-terminated self-assembled monolayers (OEG-SAMs) have intensively been studied by various techniques. However, their molecular-scale surface structure has not been well understood. In this study, we performed molecular-resolution imaging of OH-terminated SAMs (OH-SAMs) and hexa(ethylene glycol) SAMs (EG_6OH-SAMs) formed on a Au(111) surface in aqueous solution by frequency modulation atomic force microscopy (FM-AFM). The results show that most of the ethylene glycol (EG) chains in an EG_6OH-SAM are closely-packed and well-ordered to present a molecularly-flat surface even in aqueous solution. In addition, we found that EG_6OH-SAMs have nanoscale defects, where molecules take a disordered arrangement with their molecular axis parallel to the substrate surface. We also found that the domain size (50–200 nm) of an EG_6OH-SAM is much larger than that of OH-SAMs (10–40 nm). These findings should significantly advance molecular-scale understanding on the surface structure of OEG-SAMs.

PACS numbers: 07.79.Lh, 68.37.Ps

1. Introduction

Surfaces coated with poly(ethylene glycol) (PEG) exhibit strong resistance to nonspecific protein adsorption (i.e. protein resistance). Owing to this property, they are widely used in biomedical and biosensing applications. Examples include coatings of substrates for cell culture, contact lenses, catheters and biosensors.[1–7] To improve the protein resistance of the coatings, tremendous efforts have been made for understanding the mechanism and optimizing the coating conditions. In these studies, oligo(ethylene glycol)-terminated alkanethiol self-assembled monolayers (OEG-SAMs) have widely been used as a model system.[8–12]

In contrast to a PEG film, an OEG-SAM consists of monodisperse molecules with uniform chain length. Thus, the interface between the molecules and water is well-defined. In addition, an OEG-SAM offers excellent controllability of the physical and chemical properties of the surface. The lateral packing density can be controlled by changing the substrate (e.g. Au and Ag) used for preparing a SAM.[10,13] Further control of the conformational flexibility can be achieved by mixing alkanethiols with and without ethylene glycol (EG) chains.[9,14] The affinity to water can be modified by changing the end group of the EG chains (e.g. OH and OCH_3).[13,15,16] Such an excellent controllability makes the system ideal for studying molecular-scale mechanism of the protein resistance.

In an effort to understand the origin of the protein resistance of OEG-SAMs, their molecular arrangements and conformations have extensively been studied by various spectroscopic techniques.[17–20] In the meanwhile, microscopic studies on the surface structures of OEG-SAMs have been very limited. In particular, molecular-scale arrangements of domain boundaries, etch pits and defects of an OEG-SAM have not been well understood. This has often hindered understanding relationship between the protein resistance and the local surface structures.

Atomic force microscopy (AFM)[21] is a powerful tool for imaging molecular-scale surface structures in liquid. Among various operation modes of AFM, static or amplitude-modulation mode has typically been used for liquid-environment imaging. For example, Li *et al.* used these operation modes for investigating chain length dependence of surface structures of OEG-SAMs.[20] The obtained images revealed that the surface roughness of an OEG-SAM increases with increasing the length of EG chains. However, molecularly-resolved AFM images of an OEG-SAM have not been reported yet. This is partially due to the difficulties in reproducible and non-destructive imaging of soft surface structures with molecular resolution in liquid.

Recently, there have been significant advancement in high-resolution imaging techniques using dynamic-mode AFM in liquid. Frequency modulation AFM (FM-AFM)[22] has traditionally been used for atomic-scale investigations in vacuum.[23,24] However, recent progress in the instrumentation[25] has enabled its operation in liquid with atomic resolution.[26] One of the key techniques that brought this breakthrough is ultra small amplitude oscillation of a cantilever (< 0.5 nm). Subsequent studies revealed that the small amplitude operation is also effective to improve spatial resolution of AM-

AFM in liquid.[27] Another method proposed for high-resolution imaging in liquid is bimodal AFM.[28] In the method, the first and second vibration modes of a cantilever are simultaneously excited. Typically, oscillation amplitude of the second mode is set at a small value to obtain atomic-scale locality in the force detection.

Among these advanced AFM techniques, here we use FM-AFM for investigating surface structures of OEG-SAMs. We perform molecular-scale FM-AFM imaging of OH-terminated alkanethiol SAMs with and without hexa(ethylene glycol) chains (EG_6OH-SAMs and OH-SAMs) in NaCl solution. By comparing the images of these two systems, we aim at understanding the influence of the EG chains on the surface structure. In particular, variations in the molecular-scale contrast patterns are discussed in detail.

2. Experimental details

2.1. Sample Preparation

Au(111) surface was prepared by vacuum deposition of gold onto a mica substrate (01877-MB, SPI Supplies). We cleaved a mica substrate in air and introduced it into the vacuum chamber. We performed a two-step pre-baking of the substrate at 300°C for 1h and 400°C for 1 h. With the temperature kept at 400°C, we deposited a 100 nm gold thin film on the substrate with a deposition rate of 0.1 nm/s. The vacuum pressures before and during the deposition were less than 5×10^{-5} Pa and 5×10^{-4} Pa, respectively. We performed a post-baking of the substrate at 400°C for 1 h. After the post-baking, we left the sample in vacuum until the temperature reaches room temperature. We vented the chamber with N_2 gas to take out the sample from the chamber.

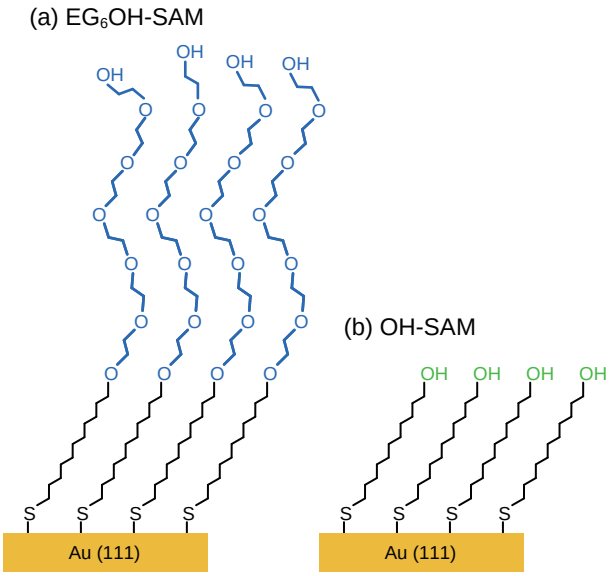

Figure 1. Schematic illustrations of (a) an EG_6OH-SAM and (b) an OH-SAM.

Immediately after taking out the substrate from the vacuum chamber, we

immersed it into a thiol solution to form a SAM. We purchased 11-Mercaptoundecanol hexaethylene glycol ether (EG_6OH-thiols) from Dojindo Molecular Technologies (H355) and 11-Mercaptoundecanol (OH-thiols) from Sigma-Aldrich (447528). The former is used for preparing EG_6OH-SAMs (Figure 1(a)) and the latter is for OH-SAMs (Figure 1(b)). We dissolved the molecules in ethanol (14722-75, Nacalai Tesque) to prepare 1 μM solutions of EG_6OH-thiols and OH-thiols. We immersed the Au(111) substrate into the solution and left it overnight in a dark room. We rinsed the substrate twice: first with ethanol and later with water. We dropped 50 mM NaCl solution (pH: $\sim$5.7) onto the SAM surface and performed FM-AFM imaging in that solution.

2.2. FM-AFM Imaging

We used a home-built FM-AFM instrument with an ultralow noise cantilever deflection sensor.[25,29] As a force sensor, we used a Si cantilever (PPP-NCHAuD, Nanoworld) with a nominal spring constant of 42 N/m. The cantilever was oscillated at its resonance frequency (f_0) with a constant amplitude (A) using a phase-locked loop (PLL) circuit (OC4, SPECS). We used the photothermal excitation method for the cantilever excitation.[29] The PLL circuit was also used for detecting the frequency shift (Δf) of the cantilever resonance induced by the tip-sample interaction. We performed FM-AFM imaging in the constant Δf mode. Namely, the tip-sample distance was regulated such that Δf was kept constant. We used a commercially available AFM controller (ARC2, Asylum Research) for the tip-sample distance regulation as well as for the scan control and the data acquisition. All the measurements were performed at room temperature in liquid.

3. Results

3.1. Surface Structures of OH-SAMs

Figures 2(a)–2(c) show FM-AFM images of an OH-SAM obtained in 50 mM NaCl solution. Note that these images are typical examples of those obtained with similar conditions. From the whole data, we confirmed that main features discussed below are reproducibe.

The micrometer-scale image (Figure 2(a)) mainly shows surface features of the Au(111) thin film formed on the mica substrate. The surface of the Au thin film shows atomically-flat terraces and large depressions formed at the boundaries between the gold grains. In the image, we also find some adsorbates with a height of 1–5 nm as indicated by the arrows. The number of such adsorbates increases with increasing the time spent for the sample transfer from the thiol solution to the imaging solution. Thus, they are probably hydrocarbon contaminations adsorbed on the surface during the sample transfer process. For OH-SAMs, we found it difficult to completely suppress such contamination.

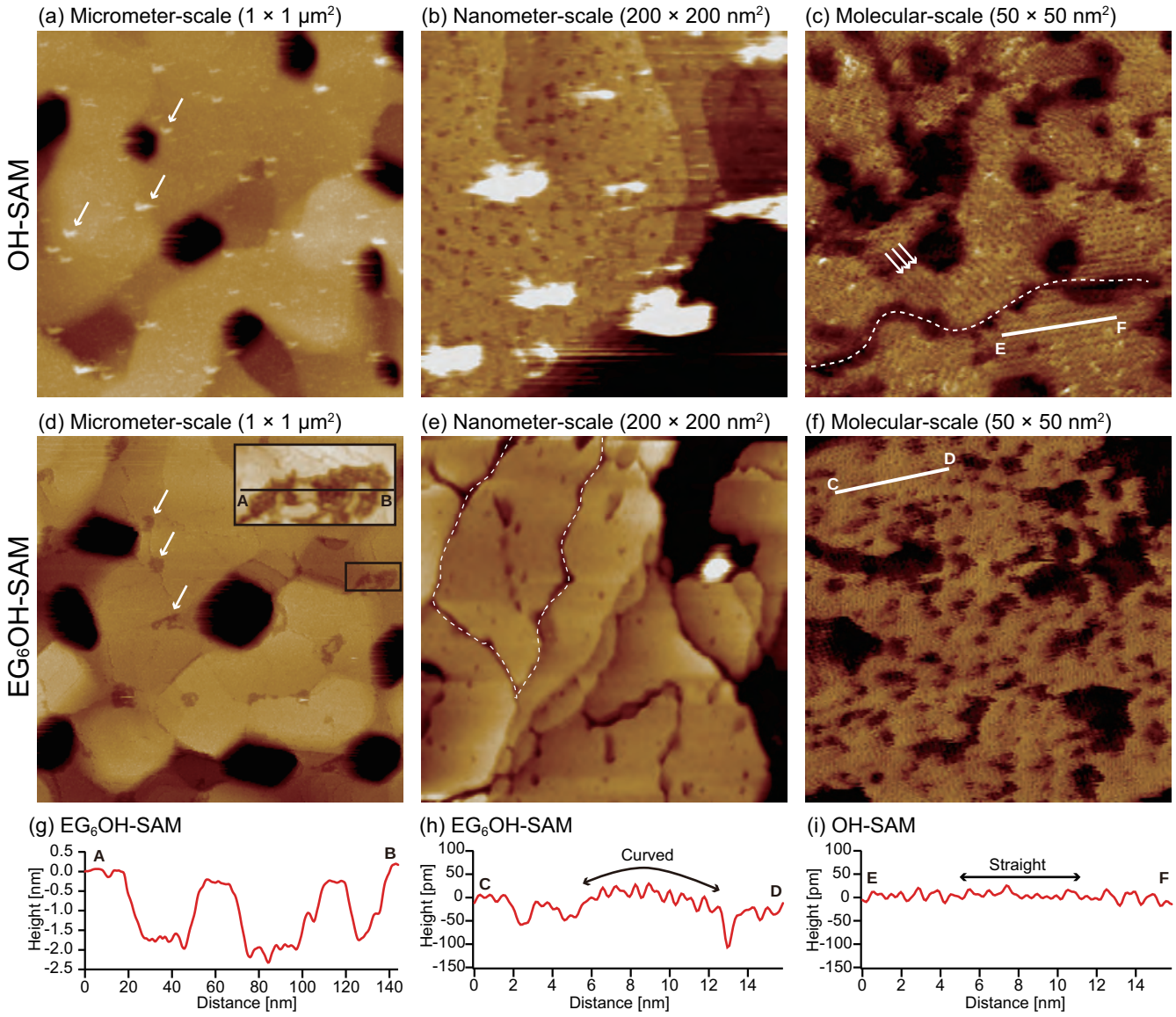

Figure 2. FM-AFM images of (a–c) OH-SAM and (d–f) EG_6OH-SAM on Au(111) surface obtained in 50 mM NaCl solution. (a) $\Delta f = +105$ Hz. $A = 0.23$ nm. (b) $\Delta f = +263$ Hz. $A = 0.23$ nm. (c) $\Delta f = +1270$ Hz. $A = 0.27$ nm. (d) $\Delta f = +98$ Hz. $A = 0.20$ nm. (e) $\Delta f = +298$ Hz. $A = 0.26$ nm. (f) $\Delta f = +327$ Hz. $A = 0.22$ nm. Cross-sectional profiles measured along Lines (g) A–B, (h) C–D and (i) E–F.

In the nanometer-scale image (Figure 2(b)), the nanoscale contaminations are more clearly observed. On the flat terraces, we find many depressions with a diameter of 2–10 nm. The depth of the depression is ∼0.25 nm, which corresponds to the single atomic step height of a Au(111) surface. Such surface structures are commonly observed at the surface of an alkanethiol SAM formed on a Au(111) surface and referred to as "etch pits".[30] In the SAM formation process, some of the thiol molecules adsorbed on the surface desorbs with a gold atom, which forms depressions with a depth corresponding to the single atomic step height. As the depressions observed in Figure 2(b) has the

characteristic height, they should correspond to the etch pits.

In the molecular-scale image (Figure 2(c)), the etch pits are more clearly observed. In addition, line-shaped depressions with a depth of 0.13 ± 0.04 nm are observed at the boundaries between two adjacent SAM domains (e.g., the depression indicated by the dotted line). On the surface of individual domains, we find two characteristic surface structures. Some domains show hexagonally-arranged molecular-scale contrasts with a spacing of 0.5 nm while the others show stripe-shaped superlattice structures with a spacing of 1 nm as indicated by the arrows in Figure 2(c). These surface structures are commonly observed at the surface of alkanethiol SAMs formed on a Au(111) surface and known as $(\sqrt{3} \times \sqrt{3})R30°$ structure and c(4×2) superlattice structure, respectively.[30,31] On the flat surfaces, we found irregularly-distributed bright spots. Their height is 50–100 pm and hence lower than that of a small molecule. Such a small contrast variation may reflect non-uniform distribution of ions, water or other molecules interacting with the surface. Complete understanding of such contrasts should require systematic studies with different ion concentrations and species.

From these results, we found that the surface structures of OH-SAMs in 50 mM NaCl solution are similar to those reported for alkanethiol SAMs in air or vacuum.

3.2. Surface Structures of EG_6OH-SAMs

Figures 2(d)–2(f) show FM-AFM images of the EG_6OH-SAM obtained in 50 mM NaCl solution. Note that these images are typical examples of those obtained with similar conditions. From the whole data, we confirmed that main features discussed below are reproducibe.

In the micrometer-scale image (Figure 2(d)), we found no contaminations on the surface. This is a clear difference from the image of the OH-SAM (Figure 2(a)). The result may reflect the non-fouling property of the EG_6OH-SAM. We also found that nanoscale depressions with a diameter of 10–50 nm exist only at the EG_6OH-SAM surface. The inset in Figure 2(d) shows an FM-AFM image taken at the area indicated by the square. The image reveals that the bottom of the depression is not atomically-flat but has irregular height variation. This suggests that the bottom is not a clean Au(111) surface but covered with adsorbed molecules. Figure 2(g) shows a cross-sectional profile measured along the line A–B indicated in the inset. The profile reveals that the depth of the depression is ∼2 nm.

According to the previous study using in-liquid IR spectroscopy, the EG chains of an OEG-SAM mostly take the helical conformation at room temperature.[32] With that conformation, the thickness of the SAM is expected to be 3.08 nm.[9] This value and the depth of the depressions (∼2 nm) suggest that the thickness of the molecular layer on the bottom should be ∼1 nm. The small thickness suggests that the film should consist of one or two molecular layers with the molecular axis nearly parallel to the Au(111) surface. From these results, we propose a model of the nanoscale defects as shown in Figure 3.

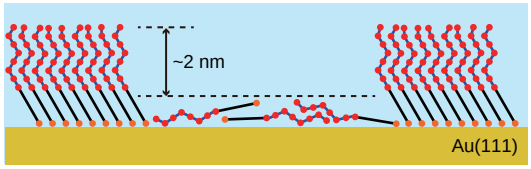

Figure 3. Schematic model of the nanoscale defects found in the EG_6OH-SAM (the arrows in Figure 2(d)).

In the nanoscale image (Figure 2(e)), we found line-shaped depressions with a depth of 0.4 ± 0.2 nm as indicated by the dotted line. Such structure is not observed in the corresponding image of the OH-SAM (Figure 2(b)). On the contrary, the molecular-scale image (Figure 2(f)) shows no line-shaped depressions corresponding to the domain boundaries. From these results, we consider that the line-shaped depressions observed in the nanoscale image should correspond to the domain boundaries. The results suggest that the domain size of the EG_6OH-SAMs is significantly larger than that of the OH-SAMs.

To obtain more quantitative information on the domain size, we performed more detailed analysis of the images (Figure 4). Figure 4(a) shows the same FM-AFM image as shown in Figure 2(c) but with domain boundaries indicated by dotted lines. We drew lines where we see a line-shaped depression, a step or a difference in the molecular contrasts between adjacent regions. Due to this definition, this process requires that the images show clear molecular-scale contrasts. Thus, the scan size was limited to less than 50 nm. Owing to this limited scan range, only three domains are completely visualized in the image. If we define the domain size as the longest edge-to-edge distance, the size of these domains is 12–32 nm.

We also performed similar analysis with other molecularly-resolved images. One of such images is shown in Figure 4(b). The largest domain found in this image has a size of ∼41 nm. This is one of the largest examples among those we analyzed. From these results, we conclude that the domain size of OH-SAMs is approximately 10–40 nm.

For EG_6OH-SAMs, we analyzed a larger image (Figure 4(c)). We drew the dotted lines where we see a line-shaped depression or a step. The molecular-scale contrasts within a single domain is almost uniform except for subtle difference discuss later with Figure 8. For example, Figure 4(d) shows molecularly-resolved images of three domains A–C. Molecular-scale contrast in each domain is almost uniform. However, across the domain boundaries, we found slight difference in the contrasts. The orientation of the molecular-scale contrasts in Domains A and C are almost the same while that of Domain B is different from the others.

In Figure 4(c), we find exceptionally small domains at the step edges. These domains exit at the step edges of the Au(111) film. Thus, their size is determined by the terrace size. Excluding these irregular domains, we find three domains that are fully included in the image. The size of these domains ranges from 64 to 170 nm.

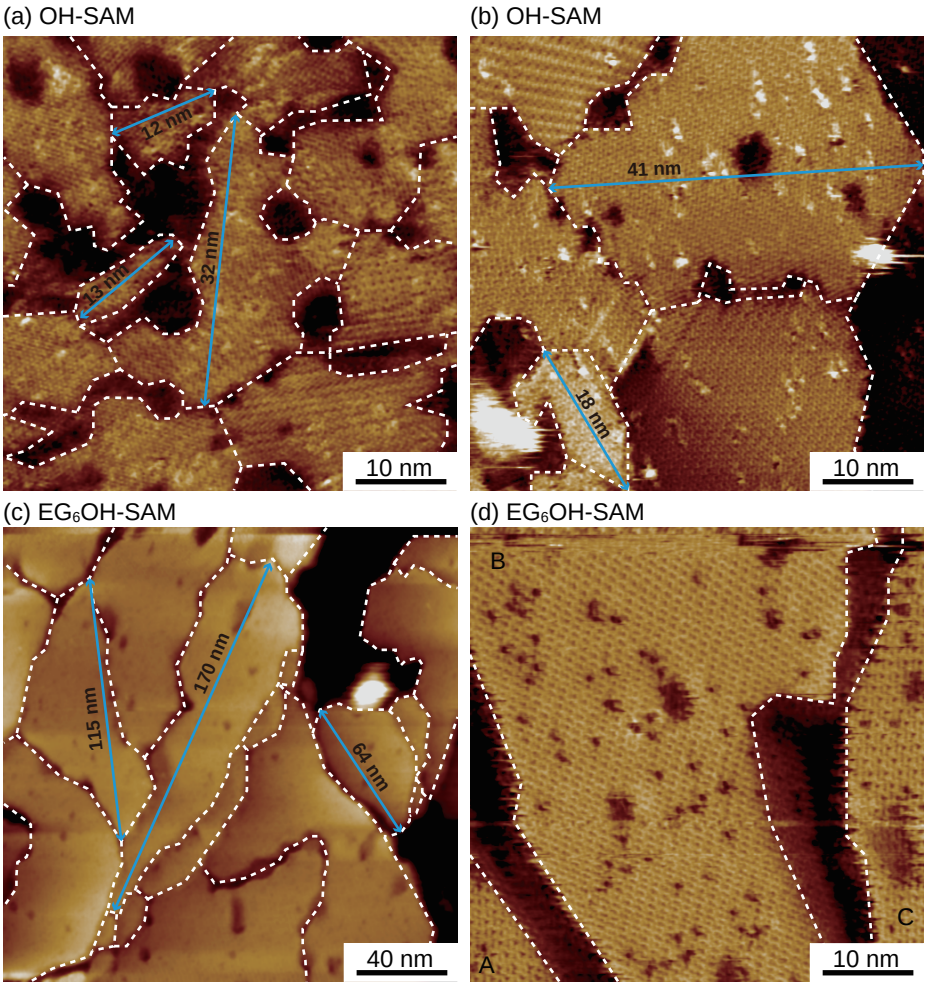

Figure 4. FM-AFM images of (a, b) OH-SAMs and (c, d) EG_6OH-SAMs obtained in 50 mM NaCl solution. (a) and (c) are the same images as shown in Figures 2(c) and 2(e), respectively. (b) $A = 0.22$ nm. $\Delta f = +93$ Hz. (d) $A = 0.17$ nm. $\Delta f = +488$ Hz. Dotted lines show approximate positions of the domain bounaries.

We analyzed other FM-AFM images obtained at different surface areas. From all the data we analyzed, we conclude that the domain size of EG_6OH-SAMs is approximately 50–200 nm. This is five times larger than that of OH-SAMs.

In the molecular-scale image (Figure 2(f)), we found depressions with different size (1–10 nm) and shape. The depth of the depressions is almost uniform and corresponds to the single step height of a Au(111) surface (∼0.25 nm). Due to the characteristic depth, they are most likely to be etch pits. However, their shape and size variation are different from those of the etch pits typically observed in alkanethiol SAMs. Thus, they may reflect non-uniform distribution of other surface structures or properties. Possible sources of such non-uniformity include the variations in the hydration properties, molecular conformations and orientations. Although we cannot exclude these possibilities, we consider that they are most likely to be etch pits as they were relatively stable during the AFM imaging.

The molecular-scale image (Figure 2(f)) shows periodic contrasts with a peak spacing of ∼0.5 nm. This value agrees with the molecular spacing observed in the $(\sqrt{3} \times \sqrt{3})R30°$ structure. The result suggests that the molecules are closely packed to form a relatively well-ordered structure. However, we found that the surface of the EG_6OH-SAM has undulation with amplitude of less than 50 pm as revealed by the cross-sectional profile in Figure 2(h). On the contrary, the OH-SAM does not show such undulation as shown by the cross-sectional profile in Figure 2(i).

In general, such subtle undulations in an AFM image can originate from sample deformation caused by the tip scan. However, we confirmed that the forward and backward scan images of Figure 2(f) show almost the same molecular-scale contrast pattern (see Figures S1(a) and S1(b) of Supplementary Data). In addition, we confirmed that successive images obtained at the same area as shown in Figure 2(f) also show a very similar contrasts (see Figures S1(a) and S1(c) of Supplementary Data). These results show that the observed undulation is not caused by the tip scan but reflects true surface topography.

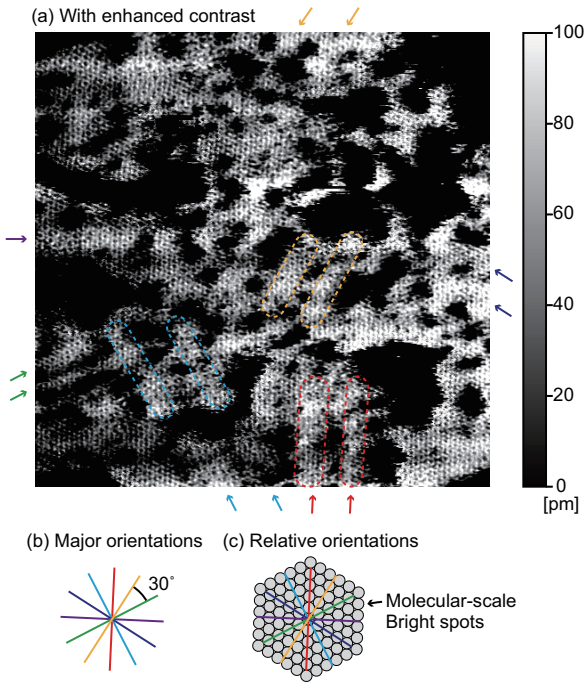

Figure 5. (a) FM-AFM image of an EG_6OH-SAM obtained in 50 mM NaCl solution. This is the same image as shown in Figure 2(f) but with an enhanced contrast. $\Delta f = +327$ Hz. $A = 0.22$ nm. Scan size: 50×50 nm^2. (b) Major orientations of the undulation stripes. (c) Relative orientations of the undulation stripes with respect to the molecular-scale bright spots observed in the image.

Figure 5(a) shows the same image as shown in Figure 2(f) but with an enhanced contrast. The image shows that the surface undulation forms stripe features with a width of 1–4 nm. The undulation stripes are mostly oriented in six major directions indicated by the arrows in Figure 5(a). The angular difference between the major

orientations is a multiple of 30° as shown in Figure 5(b). The relative orientation of these stripes with respect to the molecular-scale bright spots observed in the image is shown in Figure 5(c). These results show that the orientations of the undulation stripes have strong correlation with the molecular arrangements. Although the stripes do not have a long-range ordering, we often find small periodic structures consisting of a few stripes. Some examples are indicated by the dotted lines in Figure 5(a).

3.3. Variations in molecular-scale contrast patterns

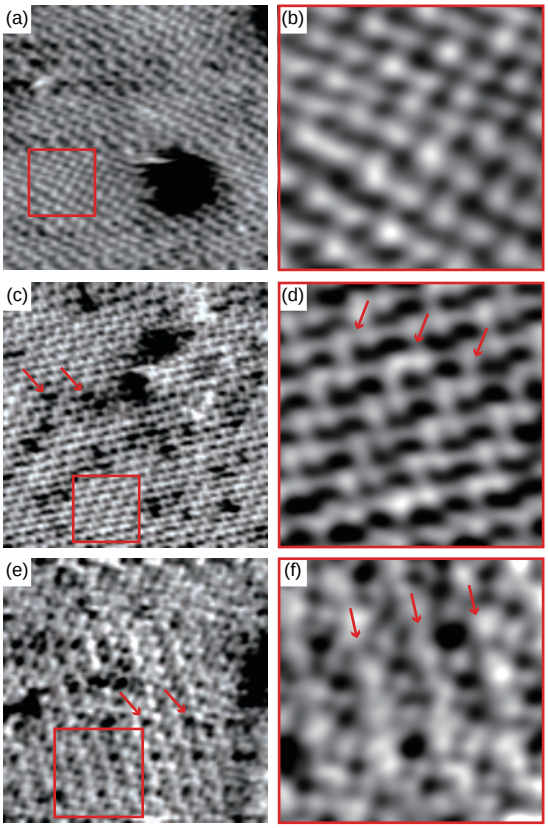

Figure 6. FM-AFM images of EG_6OH-SAMs obtained in 50 mM NaCl solution. (a) $\Delta f = +195$ Hz. $A = 0.22$ nm. 20×20 nm^2. (c) $\Delta f = +491$ Hz. $A = 0.23$ nm. 20×20 nm^2. (e) $\Delta f = +150$ Hz. $A = 0.15$ nm. 15×15 nm^2. (b), (d) and (f) are magnified images (5×5 nm^2) of the areas indicated by the squares in (a), (c) and (e), respectively.

We performed FM-AFM imaging at molecularly-flat area of EG_6OH-SAMs in 50 mM NaCl solution. The obtained FM-AFM images show various molecular-scale contrast patterns as shown in Figure 6. Molecular-scale contrasts of FM-AFM images obtained in liquid depend not only on the surface structures but also on the surface hydration structures, tip conditions and frequency shift setpoints. Thus, it is difficult to discuss the origins for the different contrasts between multiple AFM images.

Therefore, here we mainly discuss regularity and irregularity of the molecular-scale surface structures.

In the FM-AFM images shown in Figure 6(d), some domains show bright spots with a spacing of ∼0.5 nm (Figure 6(b)) while other domains show stripes with a spacing of 1 nm (arrows in Figures 6(d) and 6(f)). The latter feature is characteristic of the c(4×2) superlattice structure. These results suggest that the molecular packing arrangement in EG_6OH-SAMs is similar to that of OH-SAMs (Figure 2(c)).

However, the regularity of the molecular-scale contrasts in the images of EG_6OH-SAMs is lower than that in the images of OH-SAMs. For example, the images shown in Figure 6 show that the molecular spacing is not perfectly uniform but has variation. This is partially due to the drift of the tip position but mostly reflects real surface structures. In fact, such small variation in the molecular spacing leads to the undulation observed in the large-scale image in Figure 2(f). Another example of the irregularity is the dark spots indicated by the arrows in Figures 6(c) and 6(e). The size of these dark spots is comparable to that of the tip apex. Thus, we cannot determine if a molecule exists at these positions. Possible origins of the dark spots include missing molecules, molecular-scale etch pits, and variations in hydration or molecular conformation. Considering the strong affinity of the molecules to the Au surface and small influence on the arrangement of adjacent molecules, we speculate that the dark spots may originate from variations in hydration or molecular conformation.

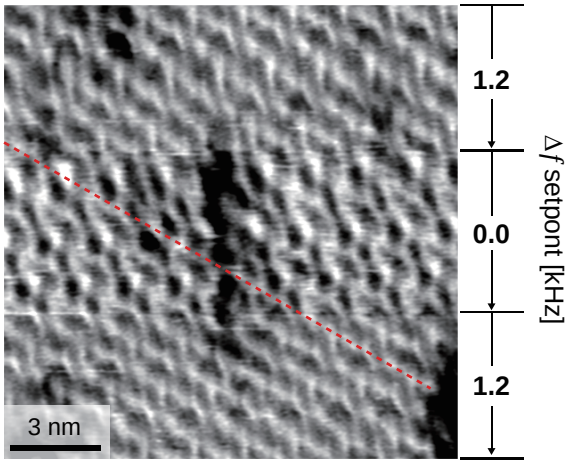

Figure 7. FM-AFM image of an EG_6OH-SAM obtained in 50 mM NaCl solution. 15 × 15 nm^2. A = 0.19 nm. During the imaging, Δf was changed from +1.2 kHz to 0 Hz and returned to +1.2 kHz.

It is generally difficult to discuss origins of the difference between molecular-scale contrasts in two AFM images. However, contrast difference in one image often provides important information on this issue. Figure 7 shows an FM-AFM image of an EG_6OH-SAM obtained with varying Δf setpoint. During the imaging, Δf was changed from 1.2 kHz to 0 Hz and returned to 1.2 kHz. Note that the FM-AFM images of EG_6OH-SAMs shown in this article were taken with a setpoint within this range. The molecular-scale

contrasts in the areas taken with 1.2 kHz and 0 Hz setpoints show a clear difference. This result shows that the molecular-scale contrast of an EG_6OH-SAM depends on Δf setpoint. However, the position of the molecular rows is not significantly shifted when Δf was changed as indicated by the dotted line in Figure 7. This result shows that the loading force during the imaging is smaller than that required for shifting the position of molecular rows.

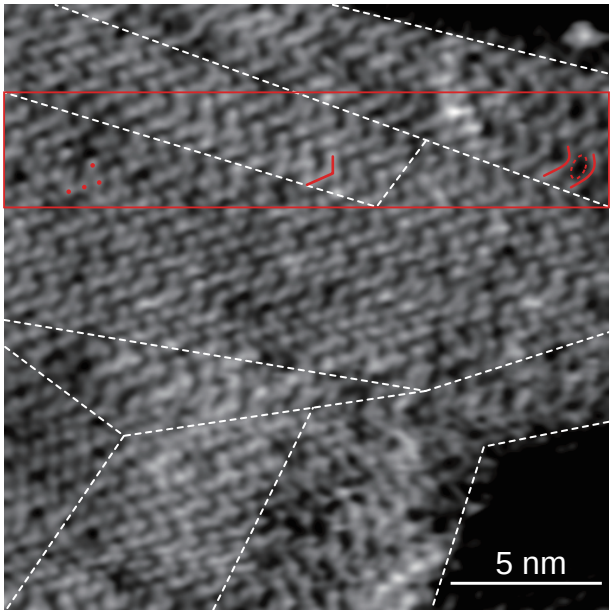

Figure 8. FM-AFM image of an EG_6OH-SAM obtained in 50 mM NaCl solution. $\Delta f = +977$ Hz. $A = 0.22$ nm.

Another example of an AFM image showing different molecular-scale contrasts is shown in Figure 8. In the image, we approximately indicated the positions of the boundaries between the areas showing different contrast patterns by dotted lines. The image shows that different contrast patterns exist even along the fast scan direction (left to right). For example, the area surrounded by the square in Figure 8 includes three regions showing different contrast patterns. In the left region, individual molecules are clearly visualized as bright spots (dots in Figure 8). In the middle region, we find characteristic L-shaped repeating units as indicated by the solid line. Molecules constituting the L-shaped features are not clearly resolved in the image. In the right region, the L-shaped units appear to be rounded to form curved lines as indicated by the solid lines in Figure 8. In addition, between two curved lines, we find a dark spot as indicated by the circle drawn with a dotted line. The difference between these characteristic features reveal the existence of different contrast patterns along the fast scan direction.

As discussed above, difference in the molecular-scale contrasts comes from the difference in surface structures, tip conditions and/or frequency shift setpoint. As for the tip conditions and frequency shift setpoint, their drift takes place along the

slow scan direction (vertical direction in Figure 8). Thus, they cannot account for the difference found between the regions along the fast scan direction. Therefore, the contrast difference should originate from the subtle difference in the surface structures. Due to the subtleness of the difference, we speculate that the difference exists only at the near surface part of the EG chains. In fact, the height difference between the areas showing different contrast patterns is less than ∼50 pm. The result suggests that the molecular conformations and orientations in these different areas are similar to each other.

4. Discussion

4.1. Nanoscale defects

In this study, we revealed the existence of nanoscale defects in EG_6OH-SAMs (Figure 2(d)). At the bottom of the defects, thiol molecules probably take a lateral orientation with respect to the Au(111) surface (Figure 3). This characteristic structure was not found in the OH-SAMs. Here, we discuss the formation mechanism of such nanoscale defects.

In general, alkanethiol molecules with a long chain length ($SH\text{-}(CH_2)_{n-1}\text{-}CH_3$; $n \geq 8$) predominantly take a vertical orientation in a SAM formed on a Au(111) surface.[33] This is partially due to the enthalpic gain obtained by the van der Waals interaction between the closely-packed alkyl chains. However, this enthalpic gain decreases with reducing the chain length. Thus, short chain molecules ($n < 8$) partially or predominantly take a lateral orientation. In this arrangement, there is an enthalpic gain obtained by the interaction between the alkyl chain and the substrate. In addition, the molecules often take a disordered arrangement to obtain an entropic gain.

For EG_6OH-SAMs, we should take into account additional energetic contributions from the EG chains. In the lateral arrangement, owing to the high conformational flexibility of the EG chains, the entropic gain obtained by the disordering is much larger than that in an OH-SAM. On the contrary, the entropic loss caused by the conformational restriction in the vertical arrangement is more significant than that in an OH-SAM. These energetic contributions can explain the coexistence of the vertical and lateral arrangements only in the EG_6OH-SAMs.

4.2. Domain size

In this study, we found that the domain size of EG_6OH-SAMs (50–200 nm) is much larger than that of OH-SAMs (10–40 nm). This size is abnormally large compared with the typical values for alkanethiol SAMs prepared with a similar procedure. Here, we discuss the formation mechanism of such large domains in EG_6OH-SAMs.

Pale-Grosdemange *et al.* performed coadsorption experiments of OH-thiols and EG_6OH-thiols and reported that OH-thiols preferentially adsorb on a Au surface.[34] The result shows that the formation of an OH-SAM is energetically preferable to that of

an EG_6OH-SAM. As discussed above, the EG chains have energetic demerits in taking the vertical molecular arrangement. Thus, an OH-SAM domain should be energetically more stable than EG_6OH-SAM domain if they have the same size.

In the formation process of a SAM, molecules first adsorb on the surface with a lateral molecular orientation.[30] Further adsorption of the molecules changes the lateral orientation to the vertical to form small domains. As the domains laterally grow, they should collide with each other to form domain boundaries. Such domain boundaries are energetically unfavorable. Thus, thermodynamically, molecules may be rearranged to form a large domain. However, such rearrangement requires disarrangement of the well-ordered molecular domains. The energy required for the disarrangement increases with increasing the domain size. Therefore, the coalescence of the domains stops at a certain domain size.

As discussed above, OH-SAM domains with the vertical molecular arrangement are energetically more stable than EG_6OH-SAM domains. Thus, the disarrangement of OH-SAM domains should require higher energy than that of EG_6OH-SAM domains if they have the same size. This explains why the domain size of EG_6OH-SAMs is abnormally large compared to that of OH-SAMs.

5. Conclusions

In this study, we imaged the surface structures of OH-SAMs and EG_6OH-SAMs in 50 mM NaCl solution by FM-AFM. Based on the obtained results and the previous reports, we have improved the understanding on the surface structures of EG_6OH-SAMs.

The surface of an EG_6OH-SAM mostly consists of closely-packed EG chains (Figure 2(f)). This result suggests that molecular conformations in an EG_6OH-SAM are almost uniform. The following features are found only in the EG_6OH-SAMs. First, we found nanoscale defects, where molecules probably take a lateral orientation. Second, the molecular-scale surface arrangement has wide variation although their difference is very subtle (Figure 8). Finally, the domain size (50–200 nm) is much larger than that of OH-SAMs (10–40 nm).

These findings have significantly improved the understanding on the surface structures of EG_6OH-SAMs. So far, such a molecular-scale study on the interfaces between soft materials and water has been hindered by the limited performance of the conventional AFM. Owing to the high spatial resolution of FM-AFM, we were able to directly visualize molecular-scale interfacial structures. This capability should also be useful in other studies on various interfacial structures. Therefore, the results obtained here should stimulate the future applications of FM-AFM to the studies on the soft interfaces in chemistry and biology.

Acknowledgments

This work was supported by KAKENHI (25706023), Japan Society for the Promotion of Science and ACT-C, Japan Science and Technology Agency.

References

[1] Valerio DiTizio, Grant W. Ferguson, Marc W. Mittelman, Antoine E. Khoury, Andrew W. Bruce, and Frank DiCosmo. *Biomaterials*, 19:1877–1884, 1998.
[2] E.L. Furness, A. Ross, T.P. Davis, and G.C. King. *Biomaterials*, 19:1361–1369, 1998.
[3] Joydeep Lahiri, Lyle Isaacs, Joe Tien, and George M. Whitesides. *Anal. Chem.*, 71:777–790, 1999.
[4] Lucio Doretti, Daniela Ferrara, Franco Schiavon, and Francesco M. Veronese. *Enzyme Microb. Technol.*, 27:279–285, 2000.
[5] N. A. Peppasa, P. Buresa, W. Leobandunga, and H. Ichikawa. *Eur. J. Pharm. Biopharm.*, 50:27–46, 2000.
[6] Fei Wang, Tatiana K. Bronich, Alexander V. Kabanov, R. David Rauh, and Jacques Roovers. *Bioconjugate Chem.*, 16:397–405, 2005.
[7] Oh Hyeong Kwon, Akihiko Kikuchi, Masayuki Yamato, and Teruo Okano. *Biomaterials*, 24:1223–1232, 2003.
[8] K. L. Prime and G. M. Whitesides. *Science*, 252:1164–1167, 1991.
[9] P. Harder, M. Grunze, R. Dahint, G. M. Whitesides, and P. E. Laibinis. *J. Phys. Chem. B*, 102:426–436, 1998.
[10] Sascha Herrwerth, Wolfgang Eck, Sven Reinhardt, and Michael Grunze. *J. Am. Chem. Soc.*, 125:9359–9366, 2003.
[11] Yi He, Yung Chang, Jason C. Hower, Jie Zheng, Shengfu Chen, and Shaoyi Jiang. *Phys. Chem. Chem. Phys.*, 10:5539–5544, 2008.
[12] Arcot R. Lokanathan, Shuai Zhang, Viduthalai R. Regina, Martin A. Cole, Ryosuke Ogaki, Mingdong Dong, Flemming Besenbacher, , Rikke L. Meyer, and Peter Kingshott. *Biointerphases*, 6:180–188, 2011.
[13] Dirk Schwendel, Reiner Dahint, Sascha Herrwerth, Matthias Schloerholz, Wolfgang Eck, and Michael Grunze. *Langmuir*, 17:5717–5720, 2001.
[14] Kevin L. Prime and George M. Whitesides. *J. Am. Chem. Soc.*, 115:10714–10721, 1993.
[15] Tomohiro Hayashi, Yusaku Tanaka, Yuki Koide, Masaru Tanaka, and Masahiko Hara. *Phys. Chem. Chem. Phys.*, 14:10196–10206, 2012.
[16] Linnea K. Ista and Gabriel P. López. *Langmuir*, 28:12844–12850, 2012.
[17] M. W. A. Skoda, F. Schreiber, R. M. J. Jacobs, J. R. P. Webstera, M. Wolff, R. Dahint, D. Schwendel, and M. Grunze. *Langmuir*, 25:4056–4064, 2009.
[18] D. Schwendel, T. Hayashi, R. Dahint, A. Pertsin, M. Grunze, R. Steitz, and F. Schreiber. *Langmuir*, 19:2284–2293, 2003.
[19] George B. Sigal, Milan Mrksich, and George M. Whitesides. *J. Am. Chem. Soc.*, 120:3464–3473, 1998.
[20] Lingyan Li, Shengfu Chen, Jie Zheng, Buddy D. Ratner, and Shaoyi Jiang. *J. Phys. Chem. B*, 109:2934–2941, 2005.
[21] G. Binnig, C. F. Quate, and Ch. Gerber. *Phys. Rev. Lett.*, 56:930–933, 1986.
[22] T. R. Albrecht, P. Grütter, D. Horne, and D. Ruger. *J. Appl. Phys.*, 69:668–637, 1991.
[23] S. Morita, R. Wiesendanger, and E. Meyer, editors. *Noncontact Atomic Force Microscopy (Nanoscience and Technology)*. Springer Verlag, 2002.
[24] Franz J. Giessibl. *Rev. Mod. Phys.*, 75:949–983, 2003.
[25] T. Fukuma, M. Kimura, K. Kobayashi, K. Matsushige, and H. Yamada. *Rev. Sci. Instrum.*, 76:053704, 2005.

[26] T. Fukuma, K. Kobayashi, K. Matsushige, and H. Yamada. *Appl. Phys. Lett.*, 87:034101–034104, 2005.

[27] K. Voïtchovsky, J. J. Kuna, S. Antoranz Contera, E. Tosatti, and F. Stellacci. *Nat. Nanotechnol.*, 5:401, 2010.

[28] T. R. Rodoriguez and R. Garcia. *Appl. Phys. Lett.*, 84:449, 2004.

[29] T. Fukuma. *Rev. Sci. Instrum.*, 80:023707, 2009.

[30] Gregory E. Poirier. *Chem. Rev.*, 97:1117–1127, 1997.

[31] Frank Schreiber. *Prog. Surf. Sci.*, 65:151–256, 2000.

[32] Stefan Zorn, Maximilian W. A. Skoda, Alexander Gerlach, Robert M. J. Jacobs, and Frank Schreiber. *Langmuir*, 27:2237–2243, 2011.

[33] M. D. Porter, T. B. Bright, D. L. Allara, and C. E. D. Chidsey. *J. Am. Chem. Soc.*, 109:3559–3568, 1987.

[34] Catherine Pale-Grosdemange, Ethan S. Simon, Kevin L. Prime, and George M. Whitesides. *J. Am. Chem. Soc.*, 113:12–20, 1991.